



OPEN Study on salt deposition distribution and environmental effect of seawater cooling tower

Lujun Li✉, Qing Zhu & Xiaojun Song

A three-dimensional numerical simulation model was developed to examine the dispersion and migration of droplets in large, naturally ventilated seawater cooling towers, as well as the pattern of salt deposition influenced by nearby buildings and crosswinds. Following a comprehensive hydrogeological survey at the site, we analyzed the effects of salt deposition on the salinity of surface water, paddy fields, and soil. Additionally, a seed planting trial was conducted to observe the growth of wheat in 11 different soil salinity conditions. The findings revealed that salt deposition did not alter the classifications of surface water quality, paddy water functionality, or soil salinization. However, soil salinity significantly affected the germination rate, bud length, bud fresh weight, and root-to-shoot ratio of the wheat variety Cangmai 6002. Assuming no erosion or dilution from rainfall, the soil salinity remained under 0.2% for 40 years, not impacting wheat yield.

Keywords Seawater cooling tower, Salt deposition, Numerical simulation, Environmental impact, Breeding experiment

Amid the rapid growth of coastal industries and the dwindling of fresh water supplies, coastal nuclear power plants increasingly rely on large seawater cooling towers with secondary cooling cycles. During operation, these towers release small, salt-containing water droplets. Due to their small size and aerodynamic properties, these droplets evade capture by water collectors and are carried outside the tower by the exhaust air, forming floating droplets. These salt-laden droplets can corrode equipment surfaces and pipelines^{1–3}, increasing anti-corrosion expenses. Additionally, when they settle on the ground, they contribute to the salinization of the soil and the withering of nearby vegetation, thus affecting the local ecology^{4–6}.

The study of the environmental impacts of floating droplets and salt deposition is crucial for the adoption of seawater cooling towers. The prediction of salt deposition in new power plants currently relies on numerical simulations. In 1972, the United States began a series of studies on floating droplets in cooling towers, leading to the development of the SACTI calculation program in 1990 by the U.S. National Laboratory Environmental Impact Research Center, using earlier models and field data^{7,8}. However, SACTI has limitations in simulating complex buildings and terrain. Recently, researchers have employed computational fluid dynamics (CFD) to analyze the flow near cooling towers, studying fog plumes and floating droplets^{9,10}. Comparing CFD and SACTI with field observations shows that CFD more accurately predicts flow fields by considering factors like fog evaporation, local circulation, and building structures, thus providing more reliable results for droplet and salt deposition¹¹.

The assessment of salt deposition's environmental impact is typically guided by the "Impact of Cooling Towers of Nuclear Power Plants" from the US Nuclear Regulatory Commission NUREG-1555, along with the "Technical Specification for Environmental Impact Assessment of Cooling Towers of Nuclear Power Plants (NB/T20307-2014)." These guidelines indicate that salt deposition levels between 100 and 200 kg/km²/month are generally harmless to plants. However, deposition exceeding 1000 kg/km²/month can damage plant leaves. The effects of deposition levels ranging from 200 to 1000 kg/km²/month on plant health remain unclear. Moreover, the severity of salt stress varies considerably among different plant varieties and developmental stages^{12–14}. For instance, under a low salt concentration (0.15%), the yield of the salt-tolerant rice varieties Yanxian 156 and Yanjing 456 increased by approximately 10%, while the yield of Yanfeng 47 decreased by approximately 16%¹⁵. It is essential, therefore, to assess the impact of salt deposition based on specific plant and crop varieties. Historically, studies on the environmental impact of cooling towers have focused predominantly on vegetation, with less attention given to the effects on surrounding soil and water.

To address this, a CFD numerical simulation model of six seawater cooling towers was developed to analyze the distribution of salt deposition and its environmental impacts, including the effects on building dynamics and

China Institute of Water Resources and Hydropower Research, Beijing 10038, China. ✉email: lilujun2008@126.com

Level	Salinity (mg/L)
Fresh water	< 1000
Brackish water	1000–3000
Saline water	3000–10,000
Salt water	10,000–50,000
Brine water	> 50,000

Table 1. Classification standard of water salinity¹⁶.

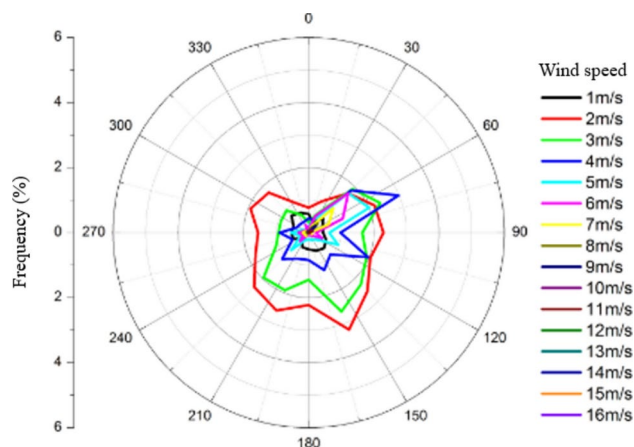


Fig. 1. Frequency distribution of wind speed and direction (Windrose).

Parameter	High level water collection cooling tower (T1–T4)	Regular cooling tower (T5–T6)
Flood area	16500 m ²	9500 m ²
Tower height	197.38 m	146.85 m
Inlet height	18.24 m	9.99 m
Throat diameter	86.3 m	65.7 m
Outlet diameter	98.4 m	74.7 m
Filler height	1.75 m	1.50 m
Shell diameter	145.95 m	110.99 m
Strut diameter	158 m	118 m

Table 2. Main dimensions of 6 cooling towers.

crosswinds. The simulation explored how salt deposition influences the salinity of surface water, water quality in paddy fields, and soil salt content. Experimental studies were also conducted to determine the effects of soil salinity on major crop growth. These findings will aid in evaluating the environmental impact of salt deposition from naturally ventilated seawater cooling towers and offer a technical reference for power plant site selection, enhancing the understanding of cooling towers' environmental impacts.

Research object

The project site is located in Jiangsu Province, China, near the Shanhou River, which has a salinity range of 981.5–1023.2 mg/L, averaging 998.8 mg/L. According to the water salinity classification standard (Table 1), the Shanhou River's surface water is classified from fresh to brackish. The area is primarily agricultural and residential, with minor industrial presence. The primary crops grown are rice in the summer and wheat in the winter.

Local climate data of 2022 from Xizou Mountain Weather Station includes an average dry bulb temperature of 16.0 °C, a wet bulb temperature of 13.0 °C, and an atmospheric pressure of 1016.6 hPa. Windroses are detailed in Fig. 1, showing hourly statistics for wind speed and direction.

The power plant houses six cooling towers, detailed in Table 2. On the west side, four high-level water collection cooling towers (T1–T4) are aligned north to south in an "I" configuration. Additionally, two standard cooling towers (T5–T6) are positioned on the east side in a similar north–south arrangement, as shown in Fig. 2. A building is situated between the two sets of towers, as indicated in Table 3.



Fig. 2. The surrounding environment of the project and the layout diagram of cooling towers and buildings in the factory.

Name	Hight	Plane size	Name	Hight	Plane size
RX	About 86	Diameter 48	UR	30.8	50.7 × 25.8
KA	51.6	37.5 × 41.7	DA	38.9	26.6 × 15.0
SX	39.5	84.3 × 62.6	DB	38.9	26.6 × 15.0
NH	36.5	58.5 × 39.7	QF	36.5	28.0 × 39.7

Table 3. Main size of buildings.

The cooling towers utilize S-wave plastic water fillers. The high-level water collection towers are designed to achieve an outlet temperature of 28.15 °C, with a wind speed of 2.01 m/s in the filler section and a circulating water volume of 46.1 m³/s per tower. The standard towers have a designed outlet temperature of 28.30 °C, a wind speed of 1.47 m/s, and a circulating water volume of 20.1 m³/s per tower. The circulating seawater in the towers has a salinity of 28‰, a concentration ratio of 1.7, and a drift rate from the water collector of 0.001%.

Methods

Control function

During stable operation of the cooling tower, the air flow inside and outside the tower is modeled under steady conditions. The flow dynamics are referenced in Zhao¹⁷. In the filler section, the fluent porous media model is used to determine resistance loss, as expressed in Eq. (1). Additionally, the discrete phase model (DPM) analyzes air resistance to raindrops in the rain zone, using Eqs. (2) to (4). The MERKEL model is applied to examine the heat exchange process between the filler and rain zone.

$$\xi_f = \frac{2A_p V^M \gamma_a}{\rho V^2 H_f} \quad (1)$$

$$\frac{d\vec{u}_p}{dt} = F_D(\vec{V} - \vec{u}_p) + \frac{\vec{g}_x(\rho_p - \rho)}{\rho_p} \quad (2)$$

$$F_D = \frac{18\mu}{\rho_p d_p^2} \frac{C_D Re}{24} \quad (3)$$

$$C_D = \frac{24}{Re} (1 + b_1 Re^{b_2}) + \frac{b_3 Re}{b_4 + Re} \quad (4)$$

where ξ_f is the resistance coefficient of filler; A_p is the experimental constant; V is the air velocity vector, m/s; M is the experimental constant; γ_a is the specific weight of air, N/m³; ρ is the density of air, kg/m³; H_f is the height of filler, m; t is the time, s; \vec{u}_p is the particle velocity vector, m/s; F_D is the drag force, N; \vec{g}_x is the acceleration vector of the particle, m/s²; ρ_p is the density of raindrops, kg/m³; d_p is the raindrop diameter, m; μ is the dynamic viscosity, Pa·s; C_D is the raindrop resistance coefficient; and bi is the experience coefficient.

The commercial computational fluid software application FLUENT solves the three-dimensional numerical model of the cooling tower. In natural ventilation towers, buoyancy is essential for the momentum equation. The modeling integrates air flow, heat transfer, raindrop evaporation, and water vapor diffusion. Variable separation solves the discrete equations, while the SIMPLEC algorithm decouples velocity and pressure. The QUICK format is used for velocity and temperature fields. FLUENT's secondary interface facilitates calculations for outer boundary conditions, filler resistance characteristics, and raindrop evaporation, utilizing user-defined functions (UDF).

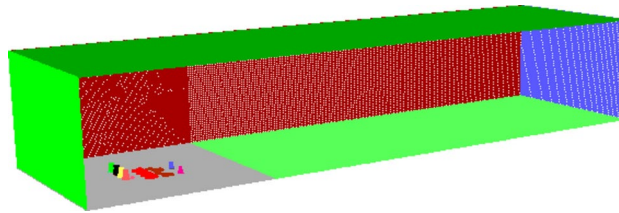


Fig. 3. Grid of the computational domain.

Particle diameter (μm)	Mass fraction (%)	Particle diameter (μ)	Mass fraction (%)
30	18.75	240	3.37
50	18.10	270	2.18
70	10.13	300	1.37
90	7.84	350	1.42
110	6.74	400	1.05
130	5.92	450	0.86
150	5.37	500	0.76
180	6.42	600	1.27
210	4.98		

Table 4. Droplet spectrum generated by cooling tower.

In this study, we calculated operating conditions involving wind speeds from 0 to 14 m/s and 16 different wind directions (from 0° to 337.5° in 22.5° increments). We conducted a weighted analysis of floating droplet sizes combined with hourly wind data to determine the distribution of salt deposition on the ground.

Grid establishment

The GAMBIT grid division software application was used to create a three-dimensional model. The computational domain measures $12,500 \text{ m} \times 4500 \text{ m} \times 2500 \text{ m}$, depicted in Fig. 3. The tower is segmented into various areas: above the throat, below the throat, filler area, bottom of the tower, and air inlet area. The grid outside the tower is sparsely distributed, while the filler area has the densest grid with approximately 8 million grids.

To track particle trajectories across different wind directions, grid models were established at 22.5° intervals between the line of towers and the far-field direction. We then calculated the 360° salt deposition around the tower group using statistical methods.

Boundary condition

The computational domain is split into two main sections: inside and outside the cooling tower. The outer region of the tower has an adiabatic boundary at the bottom, and when there is no wind, it uses a pressure outlet boundary. When there is wind, the air inlet has a velocity inlet boundary while other surfaces maintain a pressure outlet. The cooling tower's shell is adiabatically bounded, and both the inlet and outlet of the tower are treated as internal boundaries. Additionally, the filler area is considered a porous medium to establish a resistance coefficient.

Floating droplets are released from either the water collector or the throat section of the cooling tower. Their initial velocity, temperature, and quantity are defined using a discrete particle model. A droplet spectrum is outlined in Table 4 to examine motion characteristics under varying particle sizes. Equations (2) to (4) are used to calculate the trajectories of floating droplets. During the salt deposition analysis, evaporation from these droplets is ignored.

The ambient wind speed correlates with height, as defined in Eq. (5), with a wind shear index of 0.19¹⁸. A user-defined function (UDF) captures the variations in wind speed with height. The effects of ambient humidity, air moisture content, and temperature are considered at either the pressure outlet or the velocity inlet boundary.

$$v_{w,y} = v_w \left(\frac{y}{h_{ref}} \right)^{0.19} \quad (5)$$

where $v_{w,y}$ is the wind speed of height y , m/s; v_w is the wind speed of reference height, m/s; h_{ref} is the reference height, usually considered as 10 m; and y is the height, m.

Droplet data statistical method

The distribution of droplet settlement is influenced by the characteristics of droplet movement, the frequency distribution of wind, and the mass distribution of droplets. Statistically, the area around cooling towers can be

divided into several 50×50 m regions arranged on a grid, with droplet settlement assumed to be uniform in each region. The settlement in each region is calculated using Eq. (6).

$$q_i = \sum_{j=1}^{j=N} \frac{m_{d_j}}{50 \times 50 \times \rho_{d_j}} \cdot 3600 \cdot 1000 \cdot f_{d_j} \cdot f_{wind} \quad (6)$$

where q_i is the amount of droplets in the i region, mm/h; m_{d_j} is the mass of droplets with particle diameter d_j falling in this region, kg/s; ρ_{d_j} is the density of droplets with particle diameter d_j , kg/m³; f_{d_j} is the frequency of droplets with particle diameter d_j , kg/kg; f_{wind} is the wind frequency of the corresponding direction in the region.

Calculation method for salt effects on the environment

The impact of salt deposition from cooling towers on surface water, rice field water quality, and soil was analyzed using the following calculation method.

(1) Increase in surface water salinity

The increase in surface water salinity due to cooling tower salt deposition was calculated based on the Shanhou River basin area, design discharge, and salt deposition.

$$\Delta CS = \frac{A \times S_d \times 1000}{v \times 30 \times 24 \times 3600} \quad (7)$$

where A is the area of the Shanhou River, km², equal to 0.6; v is the mass flow rate of the Shanhou River, m³/s, equal to 15; S_d is the maximum salt deposition, kg/m²/month; ΔC_s is the increase in salinity, mg/L.

(2) Salt accumulation in paddy field water

Rice is cultivated once a half year in the study area, therefore the impact of salt deposition on the water quality of the paddy field is evaluated over a six-month period.

$$\Delta C_{SH} = \frac{S_d \times 6}{d_w \times 1000} \quad (8)$$

where d_w is the standing water depth of the paddy field, m, equal to 0.02–0.05, m; ΔC_{SH} is the salinity increase in half year, mg/L.

(3) Soil salt content

The increase in soil salt content caused by cooling towers on per unit area basis over T years can be calculated based on salt deposition:

$$\Delta m_s = \frac{S_d \times 12 \times T}{1000} \quad (9)$$

where Δm_s is the increase in salt content caused by the cooling tower, g/m²; and T is the accumulated time, year.

In many parts of our country, the depth of the soil layer is 30 cm. The mass of soil per unit area and the content of soluble salts can be determined using the soil's wet density and the percentage of soluble salts.

$$m_s = \rho \times d_t \times \alpha \times 1000 \quad (10)$$

where m_s is the background of salt content in soil, g/m²; ρ is the soil wet density, g/cm³, equal to 1.861; d_t is the soil layer, m, equal to 0.3; and α is the proportion of soluble salts in the soil.

Considering the increase in soil salt content and the baseline value of salt content, the soil salinity (α_T) can be computed assuming that the salt deposition from the cooling tower is considered, and the losses due to irrigation and rain erosion are excluded.

$$\alpha_T = \frac{\Delta m_s}{m_s + \Delta m_s} \times 100\% \quad (11)$$

The classification of salinization degrees, according to reference Bao¹⁹, is as follows:

- Non-salinized soil: salinity of <0.1%
- Salinized soil: salinity of 0.1–0.3%
- Medium saline soil: salinity of 0.3–0.5%
- Heavily saline soil: salinity of 0.5–1.0%
- Very heavily saline soil: salinity of >1.0%.

Experimental method for wheat salt stress

Salt deposition primarily affects the farmland of Dongxin Farm and Tongxing Town, where wheat is a key crop. Hence, the wheat variety Cangmai 6002 was selected for salt stress breeding experiments. The study examined the impact of soil salinity on the growth of Cangmai 6002 by planting 30 wheat seeds in soils with equal mass but varying salt levels.

In order to reflect the inclusion of the experiment, the soil salt content of different salt deposits (250–3000 kg/km²/month) under different cumulative years was first calculated. The maximum salt content of soil was about 0.51%. Therefore, 11 soil samples with salt content were prepared. 0.1%, 0.15%, 0.2%, ..., 0.55%, 0.6% were

tested. After pulverizing the soil, a 100 g sample is sifted through a 20 mesh/inch screen and placed in a petri dish. Sea salt is added according to the soil's salt content, and enough water is added to moisten the soil and even out the surface of the planting dish. Subsequently, 30 wheat seeds are placed in each dish and the surface is levelled again.

The moisture levels of each planting dish should be monitored daily, and appropriate watering should be conducted to maintain moisture. After 10 days, the germination rate, bud length, root length, number of roots, fresh weight of the buds, fresh weight of the roots, and the root-to-shoot ratio should be statistically analyzed using Excel and SPSS software. This experiment for each soil sample will be repeated twice to ensure accuracy.

Results

Flow field

Figure 4 illustrates the pathline of hot and humid air at the cooling tower outlet when the wind direction is 270° (west wind) and the wind speed increases from 1 to 12 m/s. At a wind speed of 1 m/s, the hot air on the windward side at the outlet of T1–T4 is deflected by the crosswind. Conversely, the hot air at the outlet of T5–T6 is drawn towards and deflected by the airflow from T1 to T4. At a wind speed of 3 m/s, the deflection of the hot air at the outlets of T1–T6 increases and is shielded by the airflow from T1 to T4, with the deflection angle at the outlets of T5–T6 being smaller than that at T1–T4. When the wind speed exceeds 5 m/s, the outlet air from the cooling tower shows significant deflection, and the deflection amplitude of the air at the outlets of T1–T6 is roughly the same.

Figure 5 shows the path of hot and moist air at the cooling tower outlet under various wind directions with an ambient wind speed of 3 m/s. When the wind direction is parallel or nearly parallel (within $\pm 22.5^\circ$) to the line connecting the towers, the airflow from T1 to T4 overlaps; for other wind directions, there is no overlap in the airflow at the tower outlets.

Droplets trajectory with different particle sizes

Figure 6 illustrates the trajectories of droplets with varying particle sizes exiting the cooling tower at a wind speed of 3 m/s and a direction of 270°. It is noted that the quantity of airborne droplets decreases as particle size increases. Particularly, at a particle size of 450 μm , droplets struggle to escape the standard tower, though they can still exit a high-level water collection tower. When particle size reaches 550 μm , escaping the high-level water collection tower becomes exceedingly difficult.

The interaction force between air and raindrops depends on their size and relative velocity of droplets. If the air velocity within the tower is too low or the droplet size too large, the droplets fail to exit the tower. Theoretical analysis indicates that droplets can only escape if Eq. (2) is greater than 0. Theoretically, at a wind speed of 2 m/s in the filler (T1–T4), the largest particle size that can exit is approximately 500 μm . Conversely, at a wind speed of 1.5 m/s in regular towers (T5–T6), the maximum particle size reduces to approximately 400 μm . These observations confirm the numerical model's accuracy in predicting droplet trajectories.

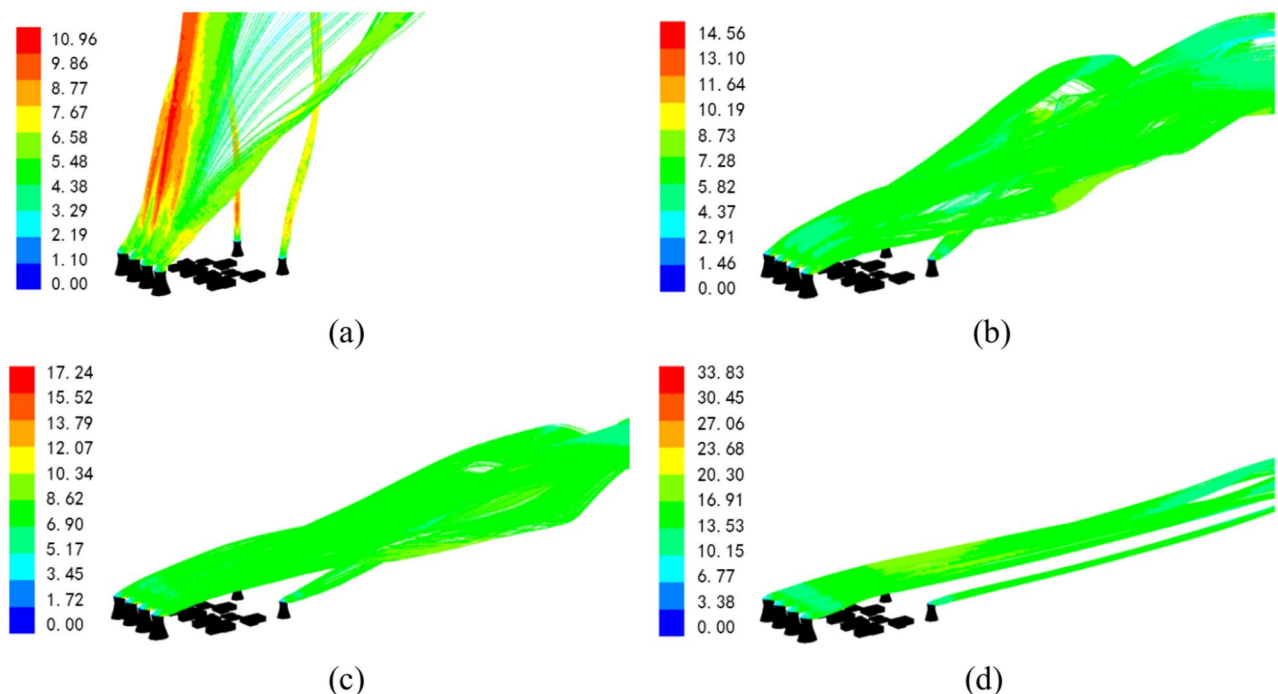


Fig. 4. Pathline when the wind direction is vertical to tower row (m/s, wind direction 270°).

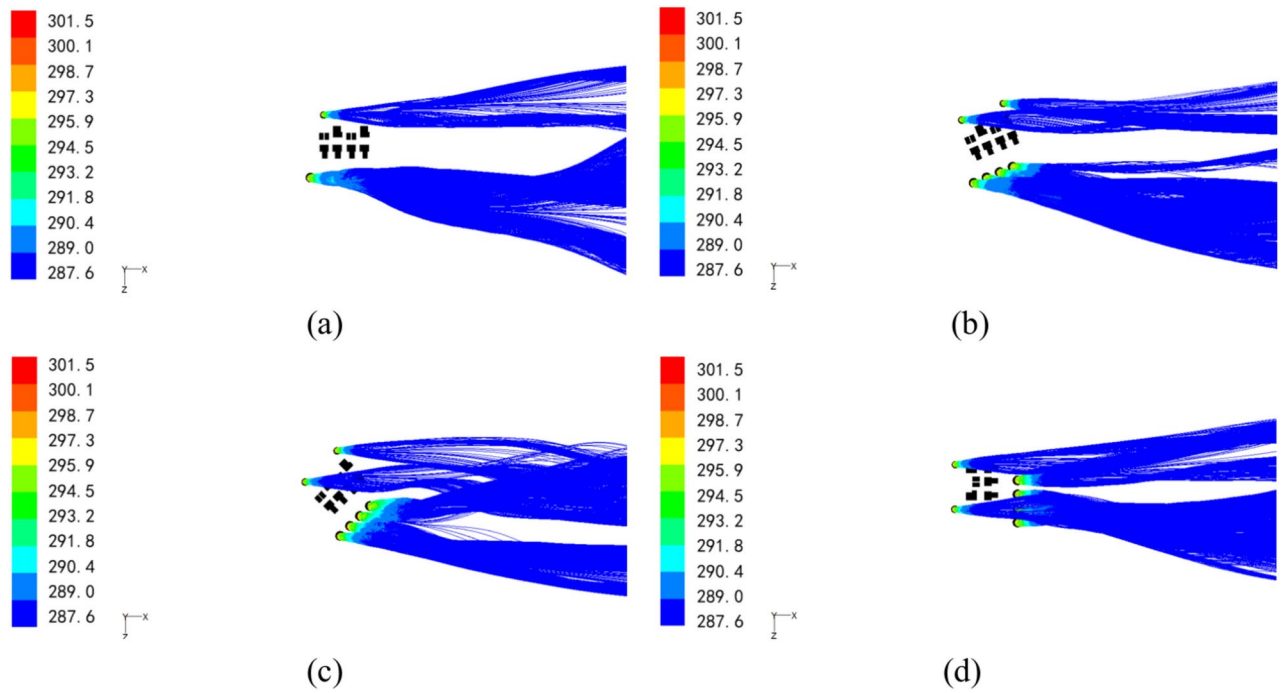


Fig. 5. Pathline from the tower outlet when the wind speed is 3 m/s (K).

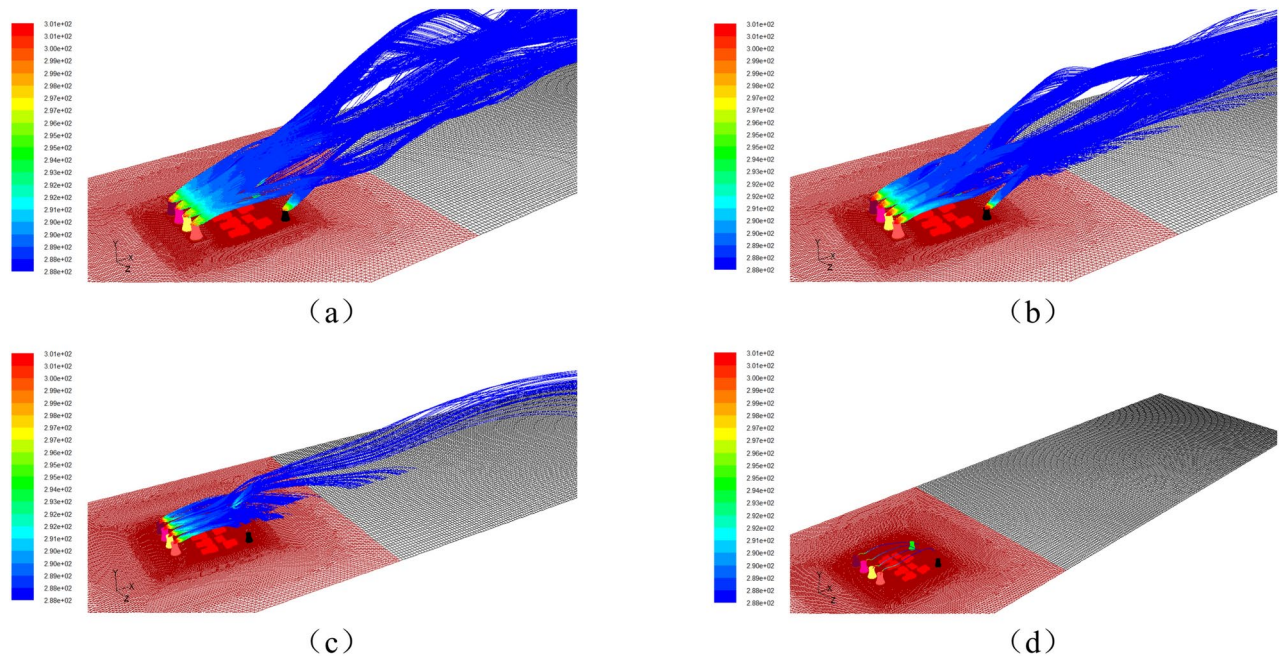


Fig. 6. Droplet trajectories of different particle diameters at cooling tower openings.

Distribution of salt deposition

As outlined in Section "Control function", monthly, seasonal, and annual salt deposition statistics were compiled, with peak values shown in Table 5. The highest salt deposition occurred in spring, totaling about 700 kg/km²/month, and the lowest in winter, at roughly 550 kg/km²/month. The highest seasonal deposition consistently occurred approximately 15° south by west, within 2.5 km of the tower center (Fig. 7). Additionally, Fig. 8 displays the annual cumulative salt distribution, with a peak of 600 kg/km²/month around 15° south by west, about 2 km from the site.

In March and July, the maximum salt deposition was 900 kg/km²/month, within safe limits. However, it remains uncertain whether this level of deposition impacts plant health in the 200–1000 kg/km²/month range.

Month	Maximum	Month	Maximum	Seasonal/annual	Maximum
Jan	530	Jul	900	Season 1 (spring)	700
Feb	800	Aug	600	Season 2 (summer)	650
Mar	900	Sep	750	Season 3 (autumn)	600
Apr	850	Oct	700	Season 4 (winter)	550
May	550	Nov	600	Annual	600
Jun	800	Dec	700	–	–

Table 5. Maximum of monthly, seasonal, and annual salt deposition ($\text{kg}/\text{km}^2/\text{month}$).

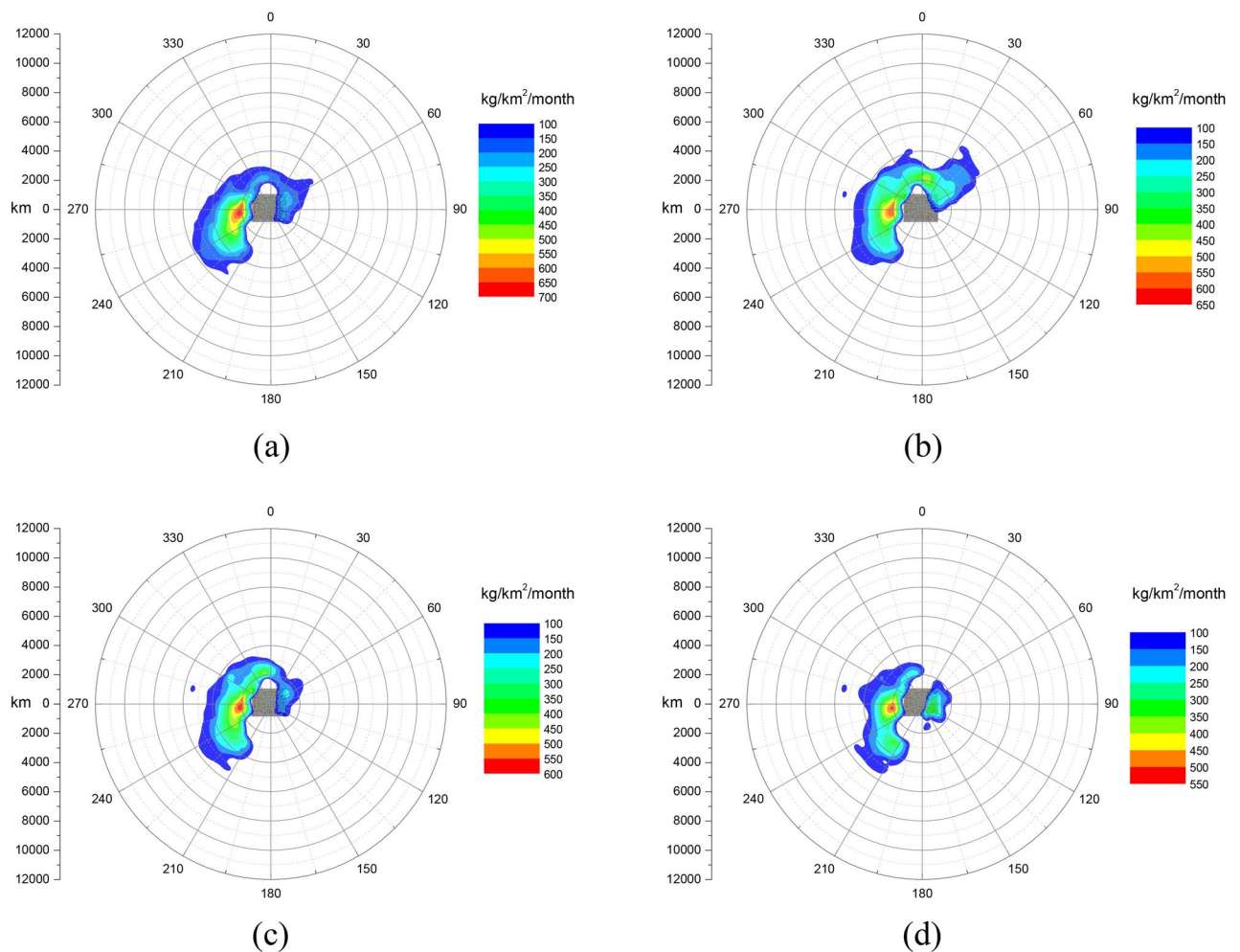


Fig. 7. Seasonal cumulative distribution of salt deposits.

Section "[Breeding experiments on the impact of soil salinity on wheat growth](#)" will detail breeding experiments to assess the effects of varying soil salinity on local plant growth.

Impact of salt deposition on the salinity of surface water

For conservative estimations, maximum values of monthly salt deposition ($900 \text{ kg}/\text{km}^2/\text{month}$), seasonal salt deposition ($700 \text{ kg}/\text{km}^2/\text{month}$), and average annual salt deposition ($600 \text{ kg}/\text{km}^2/\text{month}$) were chosen to assess the impact of cooling tower salt deposition on surface water salinity. Assuming that the dissolved salts in river water are NaCl, the increase in the salinity of river water caused by seawater cooling towers is presented in Table 6.

The cooling towers' maximum projected increase in the salinity of the Shanhou River is approximately $0.0139 \text{ mg}/\text{L}$, the effect on river salinity is less than 0.0014% , which is really small for the river. According to standard GB3838-2002, the limit for chloride (Cl^-) in surface water for concentrated drinking purposes is $250 \text{ mg}/\text{L}$, and total salinity should be less than $1000 \text{ mg}/\text{L}$. The river's average chloride concentration is about $128.6 \text{ mg}/\text{L}$, peaking at $205.3 \text{ mg}/\text{L}$, and the average total salinity is approximately $998.8 \text{ mg}/\text{L}$. Therefore, the

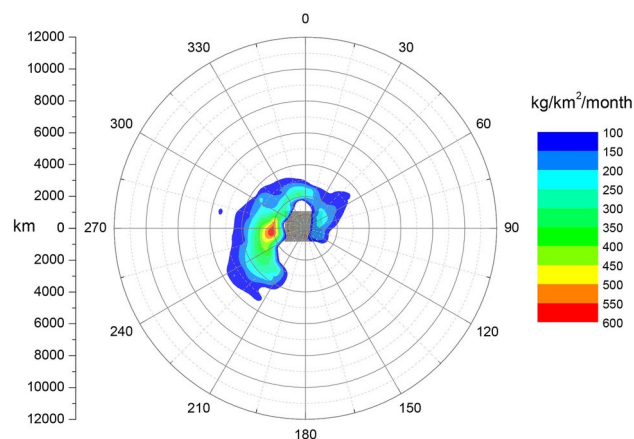


Fig. 8. Annual cumulative distribution of salt deposits.

Salt deposition (kg/km ² /month)	An increase in salinity caused by salt deposition (mg/L)	An increase rate in salinity caused by salt deposition (%)
900 (March, July)	0.0139	0.0014
700 (Spring)	0.0108	0.0011
600 (Annual)	0.0093	0.0009

Table 6. Effects of salt deposition on river channels.

Field depth (m)	Salt deposition (kg/km ² -month)	An increase in salinity at half a year (mg/L)	Total salinity at half a year (mg/L)
0.02	900 (March, July)	270	1269
	700 (Spring)	210	1209
	600 (Annual)	180	1179
0.05	900 (March, July)	108	1107
	700 (Spring)	84	1083
	600 (Annual)	72	1071

Table 7. Effects of salt deposition on the salinity of the paddy field.

cooling tower's salt deposition is unlikely to exceed regulatory limits and will minimally impact the river's water quality.

Impact of salt deposition on the salinity of the paddy field

Paddy fields irrigated by the Shanhou River assume that all dissolved salts are NaCl. The effects of maximum monthly (900 kg/km²), seasonal (700 kg/km²), and annual average (600 kg/km²) salt deposition on paddy field water salinity are shown in Table 7. Water depths of 0.02 m and 0.05 m were considered, within the typical range for paddy fields.

At water depths of 0.02 m and 0.05 m, the salinity of paddy field water can reach 1269 mg/L and 1107 mg/L respectively after 6 months. Despite the cooling tower's influence, the water quality remains within the fresh to brackish range within this period, indicating a minimal impact on salinity classification and overall water quality.

Impact of salt deposition accumulation on the salinity of soil

Based on geotechnical investigations at the plant site, it was determined that the ground is composed of silty clay with an average salinity of soluble salts at 0.12%. The wet density of the soil was measured to be 1.861 g/cm³. Following guidelines typical in China, a cultivation depth of 30 cm is recommended. The calculated soil salinity is 558 kg/m², with a soluble salt content of 670 g. It is assumed that all dissolved salts in the water are sodium chloride (NaCl). The impact of salt deposition on soil salinity was estimated using the highest average monthly salt deposition value of 900 kg/km²/month.

The local soil is categorized as salinized soil (salinity of 0.12% without the influence of cooling tower salt deposition). With salt deposition from the cooling tower, the salinity increases to 0.197% over 40 years, the salinity increases to 0.236% over 60 years, without a change in salinization degree. This estimation uses peak salt deposition values and does not account for the effects of precipitation and irrigation on reducing salinity over time, making the conclusion conservatively estimated.

Breeding experiments on the impact of soil salinity on wheat growth

Initially, the soil salt content was calculated for various deposition rates (250–3000 kg/km²/month) over different years, with a maximum recorded soil salinity of about 0.51%. Consequently, 11 soil samples with varying salinity levels (from 0.1 to 0.6%) were prepared for experimentation, as described in section "Experimental method for wheat salt stress". The growth outcomes after 10 days are depicted in Fig. 9.

From Fig. 9, it is evident that the wheat exhibits relatively high germination rates and shoot lengths at salinity levels from 0.1 to 0.2%. However, both metrics decline with increasing salinity from 0.25 to 0.35%. The trend continues, with significant reductions in germination rates and shoot lengths as salinity levels reach 0.4–0.55%. At a salinity of 0.6%, variety Cangmai 6002 fails to germinate altogether.

Table 8 illustrates the impact of varying soil salinity levels on the morphological indexes of Cangmai 6002 at the bud stage. The table uses asterisks to denote significance: * indicates a significant difference at the 0.05 level, and ** indicates an extremely significant difference at the 0.01 level. Among the 11 treatments, there were significant or extremely significant differences in germination rate, bud length, bud fresh weight, and root-to-shoot ratio, while the other three morphological indexes showed no significant differences.

Table 9 presents the results of multiple comparisons where the same letter denotes no significant differences, and different letters indicate significant differences. The findings suggest that soil salinity levels between 0.10 and 0.30% do not significantly affect the germination rate, bud length, bud fresh weight, and root-shoot ratio.

In conclusion, soil salinity ranging from 0.10 to 0.20% does not impact the germination rate and bud-related indexes of Cangmai 6002 at the bud stage²⁰. A conservative analysis estimates that the maximum salt accumulation in the cooling tower deposited in the wheat field over 40 years would not significantly affect yield. According to Section "Impact of salt deposition accumulation on the salinity of soil", soil salinity is expected to reach 0.24% after 60 years of salt deposition from six cooling towers, a level at which wheat can still complete its entire growth cycle, though yield may decrease.

Given the demand in northern China for drought and alkali-resistant wheat due to their robust flavor, the higher prices of these wheat flour and related products can provide favorable economic and social benefits, potentially offsetting any production losses from drought and alkali conditions.

Conclusion

In this paper, we employ a three-dimensional numerical simulation method to examine the dynamics of floating droplets in seawater cooling towers and to quantify salt deposition. We assess the theoretical impact of salt deposition from cooling towers on the surrounding soil and water properties through numerical and mathematical analyses. Furthermore, breeding experiments were conducted to evaluate the effects of increased salinity, due to salt deposition, on wheat growth under salt stress. Our findings are summarized as follows:

- (1) Peak salt deposition occurs in March and September, reaching 900 kg/km²/month, which remains below the critical threshold for damaging plant foliage.

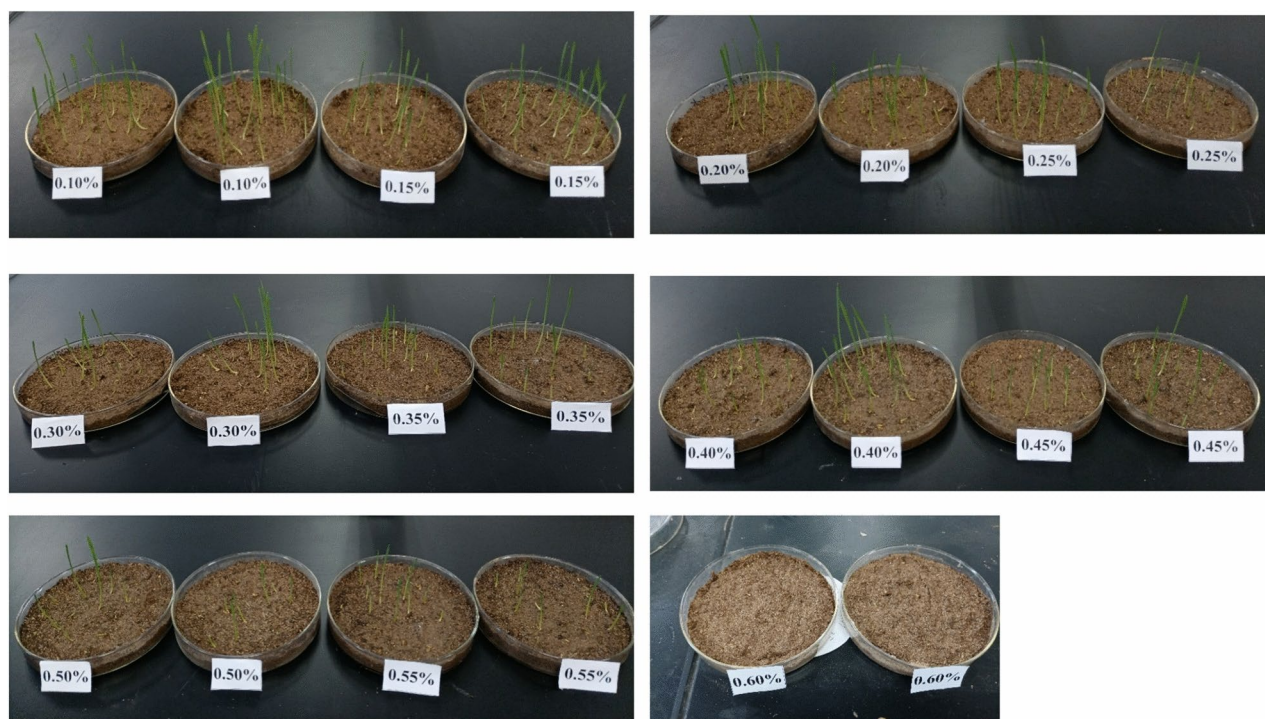


Fig. 9. Record of experimental germination of wheat with salt stress.

Mutation origin	Processing	Error	Total
df	9	10	19
Germination rate			
MS	0.0362	0.0029	
F	12.2981*		
Bud length			
MS	6.0606	1.3234	
F	4.5796*		
Root length			
MS	1.5048	0.7036	
F	2.1386		
Root number			
MS	0.1867	0.0885	
F	2.1099		
Fresh weight of bud			
MS	0.0206	0.0057	
F	3.6334*		
Fresh weight of root			
MS	0.0052	0.0033	
F	1.5845		
Root-to-shoot ratio			
MS	0.0363	0.0066	
F	5.5308**		

Table 8. Effects of soil salinity on Cangmai 6002's morphological traits. MS is mean square; F is the value of F, which is the statistic of ANOVA used to test whether the regression equation is significant.

Salt content (%)	Germination rate	Bud length (cm)	Fresh weight of bud (10 plants)	Root-to-shoot ratio
0.10	0.93a	9.62a	0.72a	0.75c
0.15	0.9ab	8.49ab	0.63ab	0.94bcc
0.20	0.88ab	8.33ab	0.63ab	0.89cc
0.25	0.83abc	6.57bc	0.53bc	0.99bc
0.30	0.78bc	6.77bc	0.52bc	0.9cc
0.35	0.75cd	7.66ab	0.53bc	0.84cc
0.40	0.73cd	6.23bc	0.54abc	0.95bcc
0.45	0.63de	6.3bc	0.54abc	0.97bc
0.50	0.58e	4.46c	0.4c	1.11ab
0.55	0.55e	4.09c	0.39c	1.23a

Table 9. Multiple comparison results of key parameters of wheat growth.

- (2) The maximum salt deposition from cooling towers, 900 kg/km²/month, raises the Shanhou River's salinity by approximately 0.0139 mg/L, maintaining its classification as fresh to brackish water.
- (3) Salt deposition increases the total salinity of paddy field water to 1269 mg/L and 1107 mg/L at depths of 0.02 m and 0.05 m, respectively, without altering its classification over 6 months.
- (4) Conservative estimates indicate that after 60 years of maximum salt deposition from cooling towers, accumulated soil salinity will remain at 0.24%, without reclassification as salinized soil.
- (5) Soil salinity levels ranging from 0.10 to 0.20% do not impact the germination rate or bud-related indices of Cangmai 6002 during the bud stage, nor do they significantly affect wheat field yield over a 40-year period despite the maximal salt accumulation from six cooling towers.

Data availability

All data generated or analysed during this study are included in this published article. All data are available from the corresponding author upon request.

Received: 5 July 2024; Accepted: 28 January 2025

Published online: 07 April 2025

References

1. Cao, M., Liu, L. & Yu, Z. Electrochemical corrosion behavior of 2A02 Al alloy under an accelerated simulation marine atmospheric environment. *J. Mater. Sci. Technol.* **35**, 651–659 (2019).
2. Leon, C. C. Anionic character of the conduction band of sodium chloride. *Nat. Commun.* **13**, 981–981 (2022).
3. Du, J. & Hesp, P. A. Salt spray distribution and its impact on vegetation zonation on coastal dunes: A review. *Estuaries Coasts* **43**, 1885–1907 (2020).
4. Schwarzenegger, A. *Performance, Cost, and Environmental Effects of Saltwater Cooling Towers* (California Energy Commission, Sacramento, 2010).
5. Rahmati, M., Alavi, S. R. & Tavakoli, M. R. Experimental investigation on performance enhancement of forced draft wet cooling towers with special emphasis on the role of stage numbers. *Energy Convers. Manag.* **126**, 971–981 (2016).
6. Alavi, S. R. & Rahmati, M. Experimental investigation on thermal performance of natural draft wet cooling towers employing an innovative wind-creator setup. *Energy Convers. Manag.* **122**, 504–514 (2016).
7. Carhart, R. A. & Policastro, A. J. A second-generation model for cooling tower plume rise and dispersion-I. Single sources. *Atmos. Pheric Environ. Part Gen. Top.* **25**, 1559–1576 (1991).
8. Carhart, R. A., Policastro, A. J. & Ziemer, S. Evaluation of mathematical models for natural draft cooling tower plume dispersion. *Atmos. Environ.* **16**, 67–83 (1982).
9. Ziqi, L. et al. Numerical simulation of deposition of drifts and salt from multiple super-large seawater cooling towers. *Sci. Rep.* **13**, 10149–10149 (2023).
10. Meroney, R. N. CFD prediction of cooling tower drift. *Wind Eng. Ind. Aerodyn.* **94**, 463–490 (2006).
11. Shi, X., Yao, R., Hu, J. & Guo, D. Comparative study on the application of CFD technology and SACTI model in local environmental impact simulation of natural ventilation cooling tower fog plume. *Radiat. Prot.* **37**, 18–26 (2017).
12. He, W. et al. Contrasting photosynthesis, photoinhibition and oxidative damage in honeysuckle (*Lonicera japonica* Thunb.) under iso-osmotic salt and drought stresses. *Environ. Exp. Bot.* **182**, 104313 (2021).
13. Zheng, Y. F. et al. Purines enrich root-associated *Pseudomonas* and improve wild soybean growth under salt stress. *Nat. Commun.* **15**, 3520–3520 (2024).
14. Yan, C. et al. Screening diverse soybean genotypes for drought tolerance by membership function value based on multiple traits and drought-tolerant coefficient of yield. *BMC Plant Biol.* **20**, 321 (2020).
15. Xu, Y. H. Effects of salt stress on different wheat varieties traits at seedling stage. *Seed* **32**, 61–64 (2013).
16. Mehdi, J. et al. Computational assessment of groundwater salinity distribution within coastal multi-aquifers of Bangladesh. *Sci. Rep.* **12**, 11165–11165 (2022).
17. Zhao, S. A. *Principle of Cooling Tower Technology* (China Construction Industry Press, 2015).
18. Chen, Y., Zhang, N. & Xu, X. The wind shear exponent in the near-surface strong wind in the coastal areas of Jiangsu Province. *Plateau Meteorol.* **38**, 1069–1081 (2019).
19. Bao, S. D. *Soil agrochemical analysis* (Beijing, 2000).
20. Wei, H. H. et al. Effects of salinity stress on grain-filling characteristics and yield of rice. *Acta Agron. Sin.* **50**, 734–746 (2024).

Acknowledgements

The authors gratefully acknowledge the scholars in the references for providing the basis for the study of salt deposition. Thanks to the computing platform provided by the author's company and the help provided by colleagues.

Author contributions

L. L.: Guarantor of integrity of entire study; Study concepts; Study design Z. Q.: Data analysis/interpretation; Statistical analysis; Manuscript revision/review S: X.: Data acquisition; Manuscript preparation; Manuscript editing.

Funding

There is no funding source.

Declarations

Competing interests

The authors declare no competing interests.

Ethical approval

This article does not contain any studies with human participants or animals performed by any of the authors.

Informed consent

Informed consent was obtained from all individual participants included in the study.

Additional information

Correspondence and requests for materials should be addressed to L.L.

Reprints and permissions information is available at www.nature.com/reprints.

Publisher's note Springer Nature remains neutral with regard to jurisdictional claims in published maps and institutional affiliations.

Open Access This article is licensed under a Creative Commons Attribution-NonCommercial-NoDerivatives 4.0 International License, which permits any non-commercial use, sharing, distribution and reproduction in any medium or format, as long as you give appropriate credit to the original author(s) and the source, provide a link to the Creative Commons licence, and indicate if you modified the licensed material. You do not have permission under this licence to share adapted material derived from this article or parts of it. The images or other third party material in this article are included in the article's Creative Commons licence, unless indicated otherwise in a credit line to the material. If material is not included in the article's Creative Commons licence and your intended use is not permitted by statutory regulation or exceeds the permitted use, you will need to obtain permission directly from the copyright holder. To view a copy of this licence, visit <http://creativecommons.org/licenses/by-nc-nd/4.0/>.

© The Author(s) 2025